International Journal of Scientific Research in Engineering and Management (IJSREM)
Volume: 10 Issue: 11 | Nov - 2026 SJIF Rating: 8.659 ISSN: 2582-3930

Study of Structural, Morphological and Optical Properties and Photocatalytic Activity of Ni Doped ZnO Nanoparticles

Jadhav Suraj Madhav

Department Of Chemistry In Shri Shivaji College Kandhar, Dist. Nanded.

Abstract:

The coprecipitation approach is used to manufacture Ni-doped ZnO nanoparticles (X=0, 0.04, 0.06). X-ray diffraction (XRD), field emission scanning electron microscopy (FESEM), energy dispersive X-ray analysis (EDX), and Fourier transform infrared spectroscopy (FTIR) techniques were used to investigate the produced nanoparticles. In Ni-doped ZnO samples with an average crystalline size of 32 nm, the XRD research revealed the hexagonal wurtzite structure of pristine and Ni-doped ZnO nanoparticles, their preferred peak growth direction the hexagonal wurtzite structure of pure and Ni doped ZnO nanoparticles, and their preferred peak growth direction is along (101) plane without inadequate phases. Nanoparticles were discovered during morphological analysis of Ni-doped samples using FESEM methods. The functional groups were investigated using FTIR and EDX to determine the elemental composition of nanoparticles. Ni-doped ZnO features wurtzite structures with NiO secondary phases, according to XRD observations and FESEM studies.

Keywords: XRD, FESEM, EDX, FTIR, Ni doped ZnO Nanoparticles

1. Introduction

Due to their potential technological uses, semiconductor nanoparticles have received a lot of attention in recent years. Because of its packaging, ZnO-based oxide semiconductors are vital for science and numerous industrial sectors. They are utilized in a variety of applications [1,2] Optoelectronics, catalysis, solar cells, an ultraviolet light emitter, a piezoelectric device, chemical gas sensors, biomedical applications, cosmetics, cells, and so on are only a few examples. As a result of surface and quantum confinement effects, new electrical, mechanical, chemical, and optical capabilities are introduced with size reduction, which is beneficial for manufacturing new generation nano-devices with excellent performance. Doping base metal oxide with various metallic elements, such as noble metals, transition metals, and metal oxides, has also been shown to be effective in this application [3,4] Fe, Cu, Cr, Co, Ni, Mn, and ZnO doped with transition metal atoms Because of its optical and electrical properties, high chemical and mechanical stabilities, and abundance in nature, ZnO has emerged as one of the most promising oxide materials researched in recent years [5,6]. ZnO is a multifunctional II-VI group semiconductor with fascinating properties such as a wide bandgap of 3.37 eV at room temperature, a large exciton binding energy of 60 meV, high optical transparency, high surface stability, large electrochemical coupling coefficient, and strong excitonic emission, to name a few [7,8]. Following the theoretical approach, DMSs displayed intrinsic room-temperature ferromagnetism, according to experimental tests. Following those experiments, interest in ni doped ZnO has grown due to its intriguing uses in spintronics, such as spin-based light-emitting diodes, sensors, and transistors, as well as its remarkable physical features [9,10]. Zhanhong Ma et al., Hydrothermal methods were used to prepare pristine and Ni-doped ZnO nanorod array films. The effects of Ni doping on the phase composition, microstructure, optical, and electrochemical characteristics of ZnO have been explored. I. Y. Habib et al., method of sol-gel Gas sensors' performance is determined by their low power consumption, quick reaction, and quick recovery times. The practical and theoretical analyses of ZnO and Cr doped materials are presented in this paper. For CO detection, ZnO nanostructures are utilized in low temperature (50 °C) sensors. XRD, UV-Vis, FE-SEM, and EDX were used to characterize the synthesized films. The creation of a single-phase hexagonal wurtzite structure is confirmed by the XRD patterns for the ZnO and 0.5 wt.% Cr/ZnO films [11,12]. A. K. Azfar et al., A sol-gel approach was used to successfully produce Ag and Ni/ZnO photocatalyst nanostructures. The photocatalyst sample was thoroughly evaluated in this study based on numerous aspects impacting photocatalyst performance, including size, shape,

bandgap, textural qualities, and the number of active sites present on the nanocatalyst surface. Wei Wang et al., At 100ºC, magnetron sputtering and hydrothermal techniques were used to create $Zn_{1-x}Ni_xO$ nanorod arrays on Si substrates. The crystal structure, morphology, photoluminescence, and magnetic characteristics of $Zn_{1-x}Ni_xO$ nanorod arrays were examined as a function of doped concentration and hydrothermal growth conditions [13, 14]. Doped ZnO has been synthesised using a variety of techniques, including sol-gel, hydrothermal combustion, and chemical vapour deposition. Except for sol-gel, all of these procedures necessitate harsh reaction conditions such as high temperatures, advanced processes, high gas purity, adjustable gas flow rate, and expensive raw ingredients, among others. As a result, the Coprecipitation method was chosen for this study due to its ease of use, mild settings, and excellent crystalline structure of the particles. The goal of this research is to use the coprecipitation approach to produce nickel-doped zinc oxide nanostructures in the most practical way possible and to characterize the nanostructures. The coprecipitation method is the simplest and most effective method for particle management. Size and morphology by systematically monitoring the reaction parameters. The obtained Ni-doped ZnO samples are hopeful candidate materials to fabricate nanoscale optoelectronic devices and sensing.

2. Experimental

All precursor materials are of high purity analytical grade. Zinc acetate dehydrate Zn $(CH_3COO)_2 \cdot 2\ H_2O)$, nickel chloride $NiCl_2 \cdot 6H_2O$ and sodium hydroxide (NaOH), were purchased from Sigma-Aldrich and distilled water were used as the solvents. Pure ZnO nanoparticles (NPs) were made by dissolving stoichiometric quantities of zinc acetate and zinc oxide separately. The same method was used to make Ni-doped samples ($Zn_{1-x}Ni_xO$ with x = 0.0, 0.04, 0.06). The synthesized zinc acetate and nickel solution was added dropwise to the resultant NaOH solution, which was then agitated constantly while heating at 60°C for 3 hours. Filtration was used to separate the precipitate from the solution, which was then rinsed multiple times with distilled water and ethanol before being dried in the air. The acquired samples were annealed for 4 hours at 500°C in a muffle furnace, after which the materials were grind in a pestal mortar until powder form.

3. Results and discussion

3.1. X-ray diffraction

The phase purity and crystal structure of the nanoparticles were determined using X-ray diffraction analysis. XRD diffraction patterns of Ni-doped ZnO nanoparticles as synthesized are shown in the figure 1. All of the diffraction peaks at angles of 31.36, 34.03, 35.86, 47.16, 56.26, 63.88, and 67.64 correspond to reflections from the zinc oxide hexagonal wurtzite crystal planes (100), (002), (101), (102), (110), (103), and (112). All of the main XRD peaks of the produced samples belong to the hexagonal wurtzite ZnO structure, as shown in Figure 1. The absence of extra peaks owing to secondary phases such as Ni metal or its oxides in Ni-doped ZnO nanoparticles was found in XRD patterns, demonstrating that the samples are Ni-doped ZnO nanoparticles. hexagonal wurtzite formations in a single phase [15,16]. The diffraction peaks with a distinct line broadening suggest that the materials are synthesized. on the nanoscale scale The average crystallite size is defined by the Debye-Scherer equation $D = 0.94\lambda/\beta Cos\theta$, which describes the link between crystal grain size and X-ray line broadening. Where, D is the average crystalline size, k is the angstrom wavelength, β is the full width at half–maximum, and θ is the Bragg angle. The sample's average crystallite size was found to be 32 nm [17].

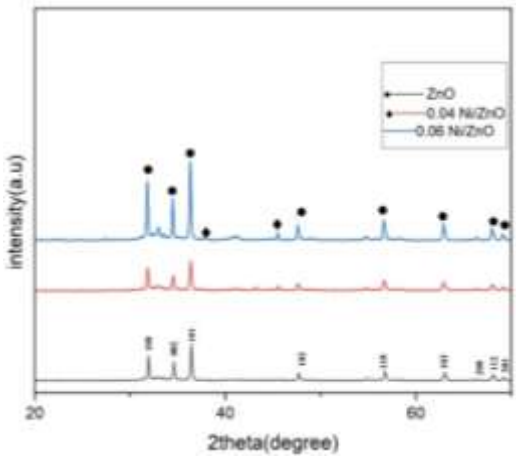


Fig 1. XRD pattern pure ZnO and Ni Doped ZnO

3.2. FESEM Analysis

The present study, displays the surface morphology of nickel-doped ZnO nanoparticles studied with field emission scanning electron microscopy (FESEM) Figure 2. shows FESEM micrographs of as-prepared nanocrystalline nickel-doped ZnO powders, whereas

Figure 2 shows FESEM micrographs of as-prepared nanocrystalline nickel-doped ZnO powders displays a magnified micrograph. In the FESEM photos, agglomeration of nanoparticles can be seen, which could be owing to the attraction forces that exist between nanoparticles when the surface area to volume ratio increases. There are also some big grains present. Figure 2. shows the morphology of $Zn_{1-x}Ni_xO$ (x = 0.0, 0.04, 0.06) nanoparticles studied using field emission scanning electron microscopy. The nanoparticles FESEM pictures reveal a uniform distribution of spherical nanoparticles with particle sizes ranging from 2µm to 200 nm [18,19].

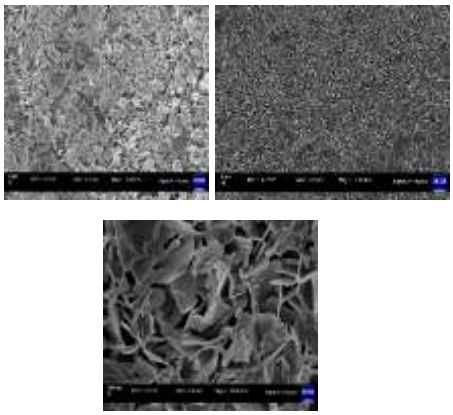


Fig 2. FESEM image pure ZnO (a) and ni doped ZnO (b and c)

3.3. EDX analysis

EDX measurements were performed on all samples to confirm the elemental distribution of pure and Ni doped ZnO nanostructures, as shown in Fig 3. The EDX results show that Zn and O are present in pure ZnO, whereas Ni, Zn, and O are present in Ni-doped ZnO nanoparticles, indicating that the nanostructures were well doped with Ni. The absence of any further impurity-related peaks in the EDX spectrum supports the samples excellent purity.

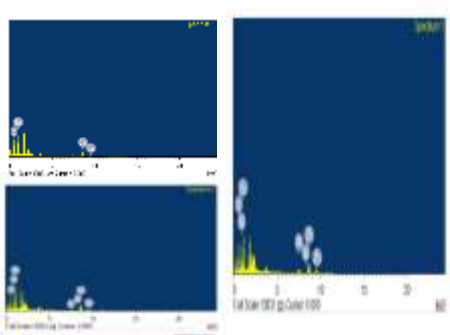


Fig 3. EDX spectra Pure ZnO (d) and Ni doped ZnO (e and f) nanoparticles

The elemental analysis of the sample was done using energy-dispersive X-ray spectroscopy (EDS). The elemental composition of nickel-doped ZnO nanoparticles as produced was determined, and the findings are presented in fig 3. This is a graph that was constructed automatically using built-in software. It belongs to the EDS spectrum. The dominant peaks for zinc, nickel, and oxygen can be seen, indicating that the produced nanoparticles were made up of these three elements. The chart also shows the percentage (percent) compositions of the elements contained in the sample. O, Ni, and Zn have weight percentages of 8.78 %, 44.79 %, and 46.43 %, respectively Similarly, O, Ni, and Zn have atomic percentages of 4.00 %, 18.34 %, and 77.66 %, respectively [20,21]. There was no other dominant peak in the spectrum, indicating that the synthesized material was in its purest form, with no other impurity elements or phases present. The EDX result confirms and verifies the XRD result, indicating that Ni-doped ZnO nanoparticles were successfully produced using the coprecipitation approach [22].

3.4. FTIR Spectra

The bands of vibrations caused by ZnO bands, as well as alterations caused by nickel doping, are studied using FTIR spectroscopy. In the region of 4000–500 cm^{-1}, FTIR spectra of pure ZnO and Ni-doped ZnO nanoparticles were observed, as shown in Fig [23]. The O–H stretching and bending vibrations of water molecules are shown by the band around 3737 cm^{-1} and the peak at 1694 cm^{-1}. The spectrum of the nickel-doped sample exhibits a drop in the intensity of the O–H band when compared to pure ZnO this can be attributed to the Ni^{2+} dopant's greater electronegative power when compared to hydrogen ions. While forming a Ni–O complex, Ni^{2+} ions were able to disrupt the O–H bond. Why the peak has dwindled dramatically CO_2 exists because of a peak at 2310 cm^{-1} caused by stretching O=C=O vibrations. Stretching C–H vibration was blamed for the band at 3398 cm^{-1}. The presence of NO_3 is responsible for the band around 1516 cm^{-1}. The presence of stretching Zn–O vibration is shown by the peaks emerging 628 cm^{-1}. At Zn^{2+} sites, the vibration modes at 632 cm^{-1} and 1007 cm^{-1} are attributable to Ni^{2+} occupancy. When compared to pure ZnO, these results exhibited some differences. The difference in ionic radii of Zn^{2+} and Ni^{2+}, which enables the substitution of Zn^{2+} by Ni^{2+}, may explain the existence of a frequency shift between the two spectra [24,25].

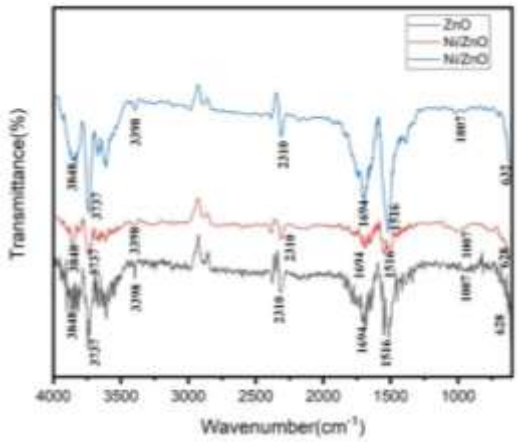


Fig 4. FTIR Spectra Pure ZnO and Ni doped ZnO nanoparticles

UV-Visible spectroscopy

Ni doped ZnO nanoparticles that had just been produced were suspended in ethanol to measure UV absorption spectra. Ethanol was utilised in this experiment as a reference standardisation before the measurement. As can be seen in Fig. 4, these samples' UV-visible absorption spectra were studied in the 300 to 800 nm region.

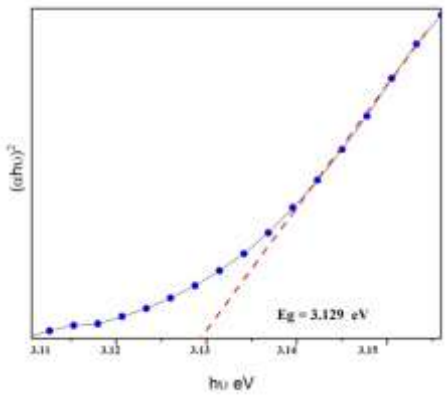


Fig. 4 Absorption spectra with calculated bandgap of Ni doped ZnO nanoparticles

.5 Photocatalytic activity

Using the formula shown below, the percentage of degradation was computed.

$$\%\, Degradation = \frac{C_0 - C_t}{C_0} \times 100$$

Where, C_0 = initial absorbance of MB Dye, C_t = absorbance after 20 min interval of time (t).

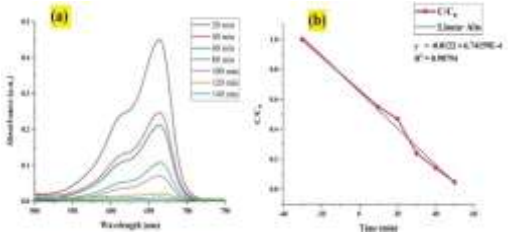


Fig. 7 (a) Time-dependent UV–Vis absorption spectra of green synthesized Ni doped ZnO nanoparticle with Rhodamine B dye under sunlight (b) Degradation of RB dye solution as a function of different time intervals.

The graph shown in figure 5 (a), shows that the linear trend between methylene blue dye versus time provides the rate constant equal to (y = -0.0122 6.74159E-4) and R square is close to 1 that is $R^2 = 0.98794$.

Photocatalytic Degradation Mechanism

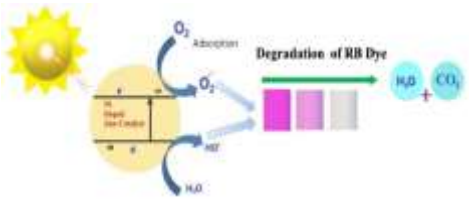


Fig. 2 Photocatalytic reaction mechanism

When Ni doped ZnO nanoparticles are exposed to sunlight, the excitation of an electron from the second conduction band leaves the holes in the valence band with some additional energy, helping to promote the formation of hole electron pairs. The Ni doped ZnO nanoparticle develops a positively charged surface that interacts with the electrons in the surrounding liquid. Superoxide anions are created when the reaction between an excited electron and oxygen in a group-prepared nanoparticle separates the water molecule to form a hydroxyl radical. The breakdown of the Rhodamine B dye is accomplished through oxidative destruction using the hydroxyl radical and superoxide anion. The created nanoparticles are effective degradation catalysts.

Conclusion

The Co-Precipitation process was used to make Ni-doped ZnO nano-crystalline ($Zn_{1-x}Ni_xO$), where x = (0.0,0.04,0.06) nanoparticles. The effects of doping concentrations on their structural and morphological features were examined. As the doping ratios were increased, the size of the nanoparticles diminished. The

hexagonal wurtzite structure is shown by XRD examination, and the typical crystallite size is estimated to be between 32 nm. The morphology of the obtained undoped and Ni-doped ZnO nanoparticles is found to be flower like structures, according to FESEM measurements. The quality of the purity undoped and Ni-doped ZnO nanoparticles is confirmed by EDX analysis. The chemical bonding and functional groups of produced nanostructures were investigated using FTIR bands, which were found in the range of 4000–400 cm^{-1} for all nanostructures. All These nanoparticle properties, such as Ni doped ZnO nanoparticles, appear to be ideal for sensing devices, lasers, and photovoltaic applications.

References

1) Doğan, N., Ayhan Bingölbali, and L. Arda. "Preparation, structure and magnetic characterization of Ni doped ZnO nano-particles." Journal of Magnetism and Magnetic Materials 373 (2015): 226-230.

2) Pal, Bappaditya, D. Sarkar, and P. K. Giri. "Structural, optical, and magnetic properties of Ni doped ZnO nanoparticles: correlation of magnetic moment with defect density." Applied Surface Science 356 (2015): 804-811.

3) Cahyaningsih, D., A. Taufik, and R. Saleh. "Effect of Ni doping on the structural and optical properties of TiO2 nanoparticles prepared by co-precipitation method." Journal of Physics: Conference Series. Vol. 1442. No. 1. IOP Publishing, 2020.

4) Srinet, Gunjan, Ravindra Kumar, and Vivek Sajal. "Structural, optical, vibrational, and magnetic properties of sol-gel derived Ni doped ZnO nanoparticles." Journal of Applied Physics 114.3 (2013): 033912.

5) Rajeh, S., et al. "Structural, morphological, optical and opto-thermal properties of Ni-doped ZnO thin films using spray pyrolysis chemical technique." Bulletin of Materials Science 39.1 (2016): 177-186.

6) Shirage, Parasharam M., et al. "Sr-and Ni-doping in ZnO nanorods synthesized by a simple wet chemical method as excellent materials for CO and CO 2 gas sensing." RSC advances 6.86 (2016): 82733-82742.

7) Ali, M. Younus, et al. "Effect of Ni doping on structure, morphology and opto-transport properties of spray pyrolised ZnO nano-fiber." Heliyon 6.3 (2020): e03588.

8) Kamble, V. S., et al. "Enhanced NO2 gas sensing performance of Ni-doped ZnO nanostructures." Journal of Materials Science: Materials in Electronics 32.2 (2021): 2219-2233.

9) Dasari, Madhava P., Umadevi Godavarti, and Vishwanath Mote. "Structural, morphological, magnetic and electrical properties of Ni-doped ZnO nanoparticles synthesized by co-precipitation method." Processing and Application of Ceramics 12.2 (2018): 100-110.

10) Al-Ariki, S., et al. "Synthesis and comparative study on the structural and optical properties of ZnO doped with Ni and Ag nanopowders fabricated by sol gel technique." Scientific Reports 11.1 (2021): 1-11.

11) Ma, Zhanhong, et al. "Structural, electrochemical and optical properties of Ni doped ZnO: Experimental and theoretical investigation." Optik 219 (2020): 165204.

12) Habib, I. Y., et al. "Enhanced Carbon monoxide-sensing properties of Chromium-doped ZnO nanostructures." Scientific reports 9.1 (2019): 1-12.

13) Azfar, A. K., et al. "Comparative study on photocatalytic activity of transition metals (Ag and Ni)-doped ZnO nanomaterials synthesized via sol–gel method." Royal Society open science 7.2 (2020): 191590.

14) Wang, Wei, et al. "Fabrication and study on magnetic-optical properties of Ni-doped ZnO nanorod arrays." Micromachines 10.9 (2019): 622.

15) Robles-Águila, M. J., et al. "Synthesis of Nanocrystalline-Doped ZnO with Al3+ and Ni2+ by Sol-Gel Method Coupled by Ultrasound Irradiation." (2018).

16) Water, Walter, Cheng-Je Li, and Liang-Wen Ji. "Application of Ni-doped ZnO nanorods in surface

acoustic wave ultraviolet photodetectors." Modern Physics Letters B (2021): 2141020.

17) Salem, Jamil K., Talaat M. Hammad, and Roger R. Harrison. "Synthesis, structural and optical properties of Ni-doped ZnO micro-spheres." Journal of Materials Science: Materials in Electronics 24.5 (2013): 1670-1676.

18) Prerna, et al. "Morphological and optical characterization of sol-gel synthesized Ni-doped ZnO nanoparticles." Integrated Ferroelectrics 205.1 (2020): 1-13.

19) Elilarassi, R., and G. Chandrasekaran. "Synthesis, structural and optical characterization of Ni-doped ZnO nanoparticles." Journal of Materials Science: Materials in Electronics 22.7 (2011): 751-756.

20) Chen, Pin-Yao, and Sheng-Hsiung Yang. "Improved efficiency of perovskite solar cells based on Ni-doped ZnO nanorod arrays and Li salt-doped P3HT layer for charge collection." Optical Materials Express 6.11 (2016): 3651-3669.

21) Kocyigit, Adem, and Ramazan Topkaya. "Structural, optical and magnetic properties of Ni-Co co-doped ZnO thin films." Materials Research Express 6.9 (2019): 096116.

22) Zou, Xiaowen, et al. "Preparation of Ni doped ZnO-TiO2 composites and their enhanced photocatalytic activity." International Journal of Photoenergy 2014 (2014).

23) Elkamel, Imen Ben, et al. "High responsivity and 1/f noise of an ultraviolet photodetector based on Ni doped ZnO nanoparticles." RSC advances 8.56 (2018): 32333-32343.

24) Cahyaningsih, D., A. Taufik, and R. Saleh. "Effect of Ni doping on the structural and optical properties of TiO2 nanoparticles prepared by co-precipitation method." Journal of Physics: Conference Series. Vol. 1442. No. 1. IOP Publishing, 2020.

25) Singh, Harpreetpal, et al. "Structural, optical and electrical properties of Ni doped ZnO nanostructures synthesized by solution combustion method." Journal of Materials Science: Materials in Electronics 29.2 (2018): 1327-1332.